Received 26 March 2021; revised 28 April 2021; accepted 10 May 2021. Date of publication 18 May 2021; date of current version 28 May 2021.
The review of this article was arranged by Editor S. Reggiani.

Digital Object Identifier 10.1109/JEDS.2021.3081463

Generalized Frequency Dependent Small Signal Model for High Frequency Analysis of AlGaN/GaN MOS-HEMTs

AAKASH JADHAV[1], TAKASHI OZAWA[2], ALI BARATOV[2], JOEL T. ASUBAR[2] (Member, IEEE), MASAAKI KUZUHARA[2] (Life Fellow, IEEE), AKIO WAKEJIMA[3] (Member, IEEE), SHUNPEI YAMASHITA[4], MANATO DEKI[4], YOSHIO HONDA[4], SOURAJEET ROY[1] (Senior Member, IEEE), HIROSHI AMANO[4] (Member, IEEE), AND BIPLAB SARKAR[1] (Member, IEEE)

1 Department of Electronics and Communications Engineering, Indian Institute of Technology Roorkee, Roorkee 247667, India
2 Department of Electrical, Electronic and Computer Engineering, University of Fukui, Fukui 910-8507, Japan
3 Department of Electrical and Mechanical Engineering, Nagoya Institute of Technology, Nagoya 466-8555, Japan
4 Department of Electrical Engineering and Computer Science, Nagoya University, Nagoya 464-8601, Japan

CORRESPONDING AUTHOR: B. SARKAR (e-mail: bsarkar@ece.iitr.ac.in)

This work was supported in part by the Indo-Japan Collaborative Science Program-2019 sponsored by the Department of Science and Technology (DST, Government of India) and Japan Society for the Promotion of Science (JSPS), Japan (Grant number JPJSBP120207711), and in part by the Science and Engineering Research Board (SERB, Government of India) under Grant SRG/2019/002092.

ABSTRACT Traditional lumped small signal equivalent circuit models of AlGaN/GaN metal oxide semiconductor high electron mobility transistors (MOS-HEMTs) are made up of constant valued circuit elements. Such models are unable to capture the high frequency behavior (above 20 GHz) of the device. In this work, a modified small signal equivalent circuit model of AlGaN/GaN MOS-HEMTs is presented. The key feature of the proposed model is that the values of the different circuit elements in the model are considered to be frequency dependent in nature and not constants. The frequency dependent value of each circuit element is mathematically represented using polynomial functions where the coefficients of the functions are determined via a least-square curve fitting approach. This frequency dependent attribute of the circuit element values ensures that the proposed model is very accurate at high frequencies without sacrificing the compactness of the model topology. The accuracy of the proposed model has been verified up to 50 GHz using experimentally measured Y-parameters of AlGaN/GaN MOS-HEMTs having a different gate dielectric and gate length.

INDEX TERMS Curve fitting, high electron mobility transistors (HEMTs), lumped model, least squares methods, unity gain frequency, Y-parameters.

I. INTRODUCTION

AlGaN/GaN high electron mobility transistors (HEMTs) are potential candidate devices to construct radio frequency (RF) electronic circuits for future 5G communications, defense, and space applications [1], [2]. Addition of a gate dielectric to realize AlGaN/GaN metal oxide semiconductor high electron mobility transistors (MOS-HEMTs) is shown to further improve the gain and noise figure of such devices when operated at high frequency [3], [4]. AlGaN/GaN MOS-HEMTs also offer a lower subthreshold leakage current, better stability, and reduced current-collapse compared to commonly used AlGaN/GaN HEMTs [5]–[7]. Traditionally, for using AlGaN/GaN HEMTs or MOS-HEMTs in RF electronic circuits, a small signal equivalent circuit (SSEC) model of the device is required. Typically, this SSEC model is generated from the measured scattering parameter (S-parameter) or Y-parameter data of the device [8]. Schematic of a conventional lumped SSEC model of an AlGaN/GaN MOS-HEMT is shown in Fig. 1 [9]–[12]. The model consists of a current source representing the drain current and few passive elements representing different resistive and capacitive elements present between the source, gate, and drain of the AlGaN/GaN HEMT or MOS-HEMT. The main advantage of this lumped SSEC model is that it enables the Y-parameters

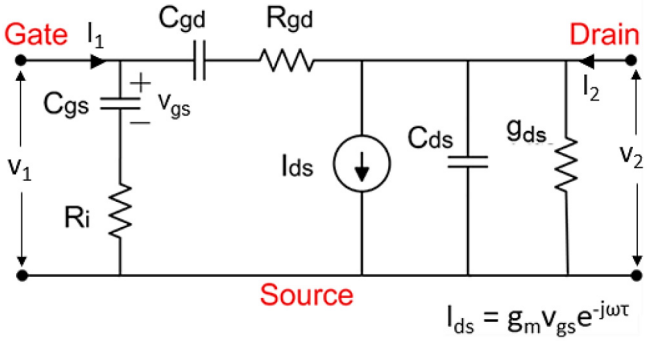

FIGURE 1. **Conventional lumped SSEC model of AlGaN/GaN MOS-HEMTs. Elements of the model are R_i, R_{gd}, g_{ds}, g_m, C_{gs}, C_{ds}, C_{gd} and τ, respectively.**

of the device to be expressed as compact closed-form functions of the values of the circuit elements of Fig. 1. Therefore, fast frequency sweeps of the device Y-parameters can be performed in an analytic manner at minimal computational time costs. Despite the above advantages of the lumped SSEC model of Fig. 1, one key limitation is that at high frequencies (i.e., generally beyond 20 GHz) this model is no longer very accurate. This is because the values of the capacitances and the transconductance element in the model of Fig. 1 are treated as constants where the constant values are extracted from low frequency Y-parameter data [13], [14]. As a result, the variation in these circuit element values at high frequency is neglected leading to modeling errors [13], [15], [16].

To mitigate the above accuracy issue, several new SSEC models have been developed for AlGaN/GaN HEMTs and other transistors by introducing additional circuit elements into the conventional SSEC model to capture the high-frequency behavior [13], [14], [17]–[21]. A two current source based SSEC model of AlGaN/GaN HEMT has also been proposed for matching the experimentally measured data [17]. However, most of these modified SSEC models of AlGaN/GaN HEMTs are empirical in nature and do not provide a generalized mechanism to improve the model accuracy. In particular, the works of [17]–[24] fail to identify a generalized strategy as to how to determine the values of the additional circuit elements. Finally, the modified SSEC models improve the accuracy of the Y-parameters at the cost of increasing the model size and complexity. Hence, the compact closed-form expressions of the Y-parameters of the device derived from the original SSEC model of Fig. 1 are no longer applicable and need to be derived anew for each modified model [17], [21].

In this work, we present a modified SSEC model of AlGaN/GaN MOS-HEMTs that is, by construction, significantly more accurate over the high frequency region of operation. The proposed SSEC model is similar in topology to the conventional SSEC model displayed in Fig. 1 with the key exception being that the values of all the circuit elements in the model are assumed to be frequency dependent and not constant. The frequency dependent circuit element values are expressed as polynomial functions of frequency and the coefficients of the functions are determined from broadband measured data using a least square curve-fitting technique. Thus, the coefficients can be determined offline. These coefficients are the new degrees of freedom introduced into the proposed model which can be tuned to capture the high frequency behavior of the AlGaN/GaN MOS-HEMT device while still preserving the simplicity of the model topology of Fig. 1. Consequently, the proposed SSEC model can still use the same compact expressions obtained from Fig. 1 to represent the Y-parameters of the device – something that is not possible for the modified SSEC models reported in [13], [14], [17]–[21]. Importantly, the proposed model is not empirical in nature and represents a general numerical approach to improve the accuracy of the conventional SSEC model of Fig. 1. The proposed model is sufficiently generic in nature, and can be applied to any field effect transistor (FET) represented using the SSEC model of Fig. 1.

In this work, the proposed model is validated using measured Y-parameter data for two different gate dielectrics and gate length values for AlGaN/GaN MOS-HEMT devices. A thorough comparison of the performance of the proposed model with respect to the conventional SSEC model of Fig. 1 is also performed in this work. This performance analysis reveals that simple 2nd order polynomial functions are sufficiently accurate to capture the frequency dependency of the circuit element values of the proposed model till 50 GHz, thereby offering far better accuracy than the conventional SSEC model of Fig. 1 at millimeter wave frequencies.

II. REVIEW OF EXISTING LUMPED SSEC MODELS FOR ALGAN/GAN MOS-HEMTS

A. REVIEW OF CONVENTIONAL SSEC MODEL

Traditionally, an AlGaN/GaN MOS-HEMT or HEMT device is treated as a two port network where the gate-to-source terminal is port 1 and the drain-to-source terminal is port 2. The measured S-parameters of this 2-port device are then converted into Y-parameters as [25]:

$$\begin{bmatrix} I_1 \\ I_2 \end{bmatrix} = \begin{bmatrix} Y_{11}(s) & Y_{12}(s) \\ Y_{21}(s) & Y_{22}(s) \end{bmatrix} \begin{bmatrix} V_1 \\ V_2 \end{bmatrix} \tag{1}$$

where Y_{11}, Y_{12}, Y_{21}, and Y_{22} represent the Y-parameters as functions of frequency and $s = j2\pi f$ where f is the instantaneous frequency. Now, by comparing the Y-parameters of equation (1) to the actual current/voltage quantities of the conventional SSEC model of Fig. 1, the following equations are obtained [25]:

$$\begin{bmatrix} Y_{11} & Y_{12} \\ Y_{21} & Y_{22} \end{bmatrix} = \begin{bmatrix} \frac{sC_{gs}}{1+sC_{gs}R_i} + Y_{gd} & -Y_{gd} \\ \frac{g_m e^{-s\tau}}{1+sC_{gs}R_i} - Y_{gd} & g_{ds} + sC_{ds} + Y_{gd} \end{bmatrix} \tag{2}$$

where

$$Y_{gd} = \frac{sC_{gd}}{1 + sC_{gd}R_{gd}} \tag{3}$$

From equation (2)-(3), the values of the individual circuit elements of the SSEC model of Fig. 1 can be represented as [25]:

$$C_{gd} = \frac{1}{\omega Im\left(\frac{1}{Y_{12}}\right)} \tag{4}$$

$$C_{ds} = \frac{Im(Y_{12} + Y_{12})}{\omega} \tag{5}$$

$$C_{gs} = -\frac{1}{\omega Im\left(\frac{1}{Y_{11}+Y_{12}}\right)} \tag{6}$$

$$R_i = Re\left(\frac{1}{Y_{11} + Y_{12}}\right) \tag{7}$$

$$g_{ds} = Re(Y_{12} + Y_{22}) \tag{8}$$

$$g_m = \left|\frac{(Y_{12} - Y_{21})(Y_{11} + Y_{12})}{Im(Y_{11} + Y_{12})}\right| \tag{9}$$

$$R_{gd} = -Re\left(\frac{1}{Y_{12}}\right) \tag{10}$$

$$\tau = \frac{\frac{\pi}{2} - phase(Y_{12} - Y_{21}) + phase(Y_{11} + Y_{12})}{\omega} \tag{11}$$

where $\omega = 2\pi f$, and Re() and Im() refers to the real part and imaginary part of the corresponding Y-parameters, respectively. From this discussion, it clear that if the measured Y-parameters of the device are known at a few frequency points, then equation (4)-(11) can be used to determine the values of the circuit elements of the SSEC model at these frequency points. For example, in [13], [14] it was demonstrated how the values of the capacitances and the transconductance element of the SSEC model can be determined from the low frequency Y-parameter data of the device. Once determined, these circuit element values can be replaced in equation (2)-(3) to predict the Y-parameters of the device at any arbitrary frequency point in the bandwidth of operation. However, it is pointed out that if the circuit element values are extracted from the low frequency region as in [13], [14], then the variation of these circuit element values with frequency, typically seen in the high frequency region, is not taken into account. Consequently, the SSEC model obtained from these circuit element values may prove to be inaccurate in the high frequency region of operation.

B. MODIFIED SSEC MODELS

Several works have attempted to address the low accuracy of the conventional SSEC model of Fig. 1 in the high-frequency region of operation. For example, Huang *et al.* enhanced the accuracy of the SSEC model by adding passive components (R_L and L_{ds}) between the drain and source terminal [21]. In particular, an inductive circuit element is added to better capture the high frequency effects of the device. A similar observation is also reported by Ahsan *et al.* where conventional constant value SSEC models of AlGaN/GaN HEMTs correctly predict the measured Y-parameters at low-frequency whereas inductive effects dominating at high frequency results in failure of the same models [13]. Adding these additional inductive circuit elements lead to greater model accuracy, but at the cost of greater model complexity. For example, the equation of Y_{22} for the modified model proposed by Huang *et al.* is given as [21]:

$$Y_{22} = \frac{\frac{1}{L_{ds}}\left(s + \frac{1}{R_{ds}C_{ds}}\right)}{s^2 + \left(\frac{R_L}{L_{ds}} + \frac{1}{R_{ds}C_{ds}}\right)s + \left(\frac{R_L}{L_{ds}R_{ds}C_{ds}} + \frac{1}{L_{ds}C_{ds}}\right)} + Y_{gd} \tag{12}$$

where separating the real and imaginary part of equation (12) becomes challenging Thus, the modified model of [21] is unable to develop any closed-form expressions similar to equations (4)-(11) to quickly determine the value of the inductive circuit element. Rather, the value of the inductive circuit element is identified using an empirical approach where the said value is tuned in a circuit simulator till an accurate fit of the predicted Y-parameters is achieved.

Another approach to better match the measured Y-parameters, proposed by Brady *et al.*, is to replace the resistive element between the drain and source terminals with a current source [17]. This modification introduces new phase elements associated with the g_{ds} circuit element shown in Fig. 1. The modified equation for Y_{22} thus becomes:

$$Y_{22} = g_{ds}e^{-s\tau_{ds}} + sC_{ds} + Y_{gd} \tag{13}$$

where τ_{ds} is an additional phase component added to match the phase component of the experimentally measured Y_{22} parameter. Unfortunately, this modification in the circuit will not increase the accuracy of the Y_{11} and Y_{12} parameters in the high frequency region. This is because these parameters are independent of the admittance branch existing between the source and drain terminals. Therefore, several such additional empirical modifications will have to be made to the circuit so as to accurately model all the Y-parameters simultaneously in the high frequency region.

In the work of Wu *et al.* [18], an additional series R-L network is introduced between the drain and source terminals of silicon-on-insulator (SOI) metal oxide semiconductor field effect transistors (MOSFETs). This R-L network is added to model the magnetic effect caused by channel current and resistive losses in silicon, respectively. Accordingly, the analytical equation of the Y_{22} parameter of the modified model of [18] changes to:

$$Y_{22} = \left(C_{ds} + C_{gd} - \frac{L_C}{R^2 + L_C^2\omega^2}\right)s + \omega^2 C_{gd}^2 R_{gd} + \frac{R}{R^2 + L_C^2\omega^2} + g_{ds} \tag{14}$$

where L_C and R are the new circuit elements added to the conventional SSEC model. However, the SSEC model of [18] only improves the low frequency (< 2 GHz) fitting of data. At frequency above 2 GHz, the circuit response is observed to be similar to that of traditionally used SSEC model.

In the work of [19], Sung *et al.* added a drain junction capacitance (C_d) and spreading resistance (R_{sub}) to capture

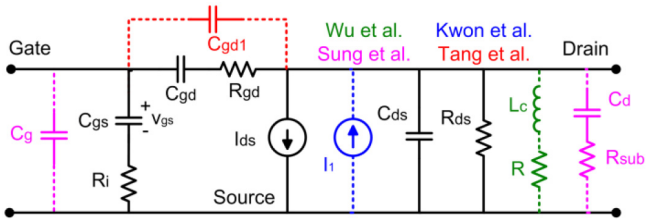

FIGURE 2. Modified SSEC models proposed by Wu *et al.* [18], Sung *et al.* [19], Kwon *et al.* [14], and Tang *et al.* [20] to match the experimentally measured Y-parameters.

the substrate coupling effects which dominates at higher frequency range in Si MOSFETs. An additional capacitance (C_g) between the gate to source terminals was also introduced to accommodate the gate-source overlap capacitance in MOSFETs. Unfortunately, it is pointed out that the addition of all these passive elements into the conventional SSEC model improves the model fit of all the Y-parameters except Y_{12}. Therefore, this modified model may still be inadequate for simulation and analysis of MOSFETs at high frequencies.

Another physics-based model was developed by Kwon *et al.* to consider the effect of charging current between the drain and gate terminals of a Si MOSFET [14]. Accordingly, a current source (I_1) was introduced between the drain and source terminals to capture the non-quasi static effects. However, introduction of the current source (I_1) results in a different value of C_{dg} given as:

$$C_{dg} = -\frac{Im(Y_{21})}{\omega} - g_m R_g (C_{gs} + C_{gd}) \tag{15}$$

where R_g represents the extrinsic gate resistance. Now, in this case, the analytical equation for Y_{21} becomes more complicated as it attempts to capture the higher order effects occurring due to the derivative of v_{gs} in the equation of I_1, that is $I_1 = (C_{dg} - C_{gd})dv_{gs}/dt$.

Finally, Tang *et al.* added an additional capacitor (C_{gd1}) between the drain and gate terminals of a MOSFET [20]. The addition of C_{gd1} helps to capture the high frequency coupling effects due to the overlap capacitance as well as the wire capacitance between the gate and drain terminals. Unfortunately, this means that the analytical equations of all the Y-parameters are different from that of equation (2) and a new set of closed-form equations similar to equation (4)-(11) need to be developed for this model. Furthermore, one additional zero gets added to the analytical equation of each Y-parameters in equation (2) resulting in further complications in the model equations.

Thus, the above discussion shows that in order to improve the accuracy of the conventional SSEC model of Fig. 1, new circuit elements must be introduced into the model, as highlighted in Fig. 2. Unfortunately, these new circuit elements will add to the model complexity, thereby ensuring that the simple expression of the Y-parameters in equation (2) and the closed-form equations of (4)-(11) are no longer applicable. In effect, new equations and empirical approaches have to be developed in order to calculate the values of the new circuit elements introduced in the model and predict the resultant Y-parameters from the model – a highly cumbersome and time-consuming task. In order to avoid this issue, generalized numerical techniques that can significantly enhance the accuracy of the conventional SSEC model of Fig. 1 in the high frequency region without disturbing its compact model topology are required.

III. PROPOSED GENERALIZED FREQUENCY DEPENDENT LUMPED SSEC MODEL

In this work, a generalized frequency dependent lumped SSEC model is developed that can accurately predict the high frequency behavior of AlGaN/GaN MOS-HEMT devices. This SSEC model possesses the same compact topology of the conventional SSEC model of Fig. 1. However, the values of the circuit elements making up this SSEC model are not assumed to be constant but rather considered to be frequency dependent in nature. In this work, the frequency dependency of the values of the circuit elements are represented using polynomial functions. Therefore, without loss of generality, any circuit element of the proposed SSEC model, say θ, can be represented as:

$$\theta(f) \approx \sum_{k=0}^{K} p_k f^k \approx p_0 + p_1 f + \cdots + p_K f^K \tag{16}$$

where K is the order of the polynomial and p_k is the k-th polynomial coefficient. Now, it assumed that the measured Y-parameters of the device are described as N sampled data points lying within the bandwidth of interest $[f_{min}, f_{max}]$ where the general i-th data point is of the form:

$$\{f_i, Y(s_i)\}; s_i = 2\pi j f_i; 1 \le i \le N; f_{\min} \le f_i \le f_{\max} \tag{17}$$

Based on the knowledge of the sampled Y-parameter data of equation (17), the value of all the circuit elements at each data point can be calculated using the closed-form expressions of equation (4)-(11). Let the calculated value of the circuit element θ at any given i-th data point be known as $\{f_i, \theta(f_i)\}$. From this knowledge, the coefficients of equation (16) for the circuit element θ will be estimated in a least square sense by solving the following over-determined system of equations [26]:

$$\boldsymbol{AX} = \boldsymbol{B}$$
$$\boldsymbol{A} = \begin{bmatrix} 1 & f_1 & \cdots & f_1^K \\ \vdots & \ddots & \ddots & \vdots \\ 1 & f_N & \cdots & f_N^K \end{bmatrix}; \boldsymbol{X} = \begin{bmatrix} p_0 \\ \vdots \\ p_N \end{bmatrix}; \boldsymbol{B} = \begin{bmatrix} \theta(f_1) \\ \vdots \\ \theta(f_N) \end{bmatrix} \tag{18}$$

where,

$$\boldsymbol{X} = \left(\boldsymbol{A}^T \boldsymbol{A}\right)^{-1} \boldsymbol{A}^T \boldsymbol{B} \tag{19}$$

Therefore, the coefficients of equation (16) can be derived for all circuit elements in the proposed SSEC model directly

from the measured Y-parameter data of equation (17). It is noted that the coefficients of equation (16) for each circuit element acts as new degrees of freedom introduced into the SSEC model. It is appreciated that these degrees of freedom were not present in the conventional SSEC model of Fig. 1. The idea is that these new degrees of freedom can be exploited to better fit the model of equation (2) to the measured Y-parameter data of equation (17) across the entire bandwidth of interest $[f_{min}, f_{max}]$ instead of only concentrating on the low frequency region of operation as done in the existing works of [13], [14], [22], [27], [28]. Therefore, in this work, the frequency dependency of the values of the circuit elements of Fig. 1, especially in the high frequency region, is not neglected and hence leads to better model accuracy.

As an additional benefit, in this work, the new degrees of freedom are introduced without changing the topology of the model of Fig. 1. This ensures that the Y-parameters of the device can be predicted at any arbitrary frequency point by using the same compact expressions of equation (2) with the only modification being that now the circuit element values in equation (2) are no longer treated as constants but rather as polynomial functions of frequency as:

$$\begin{bmatrix} Y_{11}(f) & Y_{12}(f) \\ Y_{21}(f) & Y_{22}(f) \end{bmatrix} = \begin{bmatrix} \frac{sC_{gs}(f)}{1+sC_{gs}(f)R_i(f)} + Y_{gd} & -Y_{gd} \\ \frac{g_m(f)e^{-s\tau(f)}}{1+sC_{gs}(f)R_i(f)} - Y_{gd} & g_{ds}(f) + sC_{ds}(f) + Y_{gd} \end{bmatrix};$$
$$Y_{gd} = \frac{sC_{gd}(f)}{1 + sC_{gd}(f)R_{gd}(f)} \quad (20)$$

where the polynomial functions of equation (20) have already been determined using the least-square curve-fitting technique of equations (18)-(19). Thus the ability of the proposed frequency dependent SSEC model to directly utilize the equation (2) in order to predict the Y-parameters of the AlGaN/GaN MOS-HEMT device represent a clear advantage over the reported works of [14], [18]–[21]. This is because in the reported works of [14], [18]–[21], additional new circuit elements are added into the SSEC model of Fig. 1. The addition of these new circuit elements complicates the model topology of Fig. 1, thereby necessitating the derivation of a new set of expressions for the Y-parameters of the device as opposed to directly using equation (2).

IV. EXPERIMENTAL DETAILS

A key aspect of this work is to use experiments to measure the Y-parameters of fabricated AlGaN/GaN MOS-HEMT devices. It is this measured Y-parameters that is latter used in the curve fitting approach of equations (18)-(19) of the proposed frequency dependent SSEC model. In this section, the details of the experiments performed and the device structures studied in order to measure the Y-parameters is provided. The AlGaN/GaN hetero-structures used in this work is grown on 4H-SiC substrates and procured from commercial vendors. The hetero-structure consist of a 500 nm thick un-doped GaN layer and a 25 nm thick $Al_{0.25}Ga_{0.75}N$ barrier layer. Schematic of the fabricated AlGaN/GaN MOS-HEMTs are shown in Fig. 3. The fabrication includes a mesa isolation performed using an inductively coupled plasma reactive ion etching (ICP-RIE) system. Source/drain ohmic contacts are then formed by depositing Ti/Al/Mo/Au (15/60/35/50 nm) using e-beam evaporation system under high vacuum followed by rapid thermal annealing (RTA) at 860 $^{\circ}C$ for 30 sec in N_2 environment. Subsequently, a 10 nm thick gate dielectric deposition is done where the gate dielectric is chosen to be either SiO_2 deposited using RF sputtering or Al_2O_3 deposited using atomic layer deposition (ALD) system. Standard Ni/Au (50/150 nm) Schottky gate contacts are then deposited using e-beam evaporation system. Gate width of the AlGaN/GaN MOS-HEMTs are kept to be 100 μm, whereas gate length (L_G) is set to two specific value of $L_G = 2$ µm and $L_G = 1.5$ μm. In effect, four different devices are fabricated for the Y-parameter measurements – one each with SiO_2 and Al_2O_3 gate dielectric of channel length $L_G = 2$ µm and $L_G = 1.5$ μm. For each device, silicon nitride passivation dielectric (150 nm) is deposited using sputtering system. All the devices in this study has a gate to drain and gate to source distance of 6 μm and 2 μm, respectively.

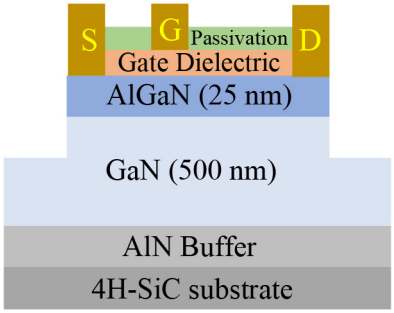

FIGURE 3. Cross-sectional schematic of AlGaN/GaN MOS-HEMTs investigated in this work.

S-parameter characterization of all the devices are carried out for a frequency range of [300 MHz, 50 GHz] (i.e., $f_{min} = 300$ MHz and $f_{max} = 50$ GHz) at drain-to-source voltage (V_{DS}) = 15 V and gate-to-source voltage (V_{GS}) is set to the value when transconductance is maximum measured using a network analyzer. A total of $N = 498$ sample points is used in the S-parameter characterization. Short circuit and open circuit tests were performed for the devices in order to evaluate the intrinsic S-parameters (or Y-parameters) based on open-short de-embedding method to eliminate the pad reactance and interconnect reactance [29], [30]. The S-parameters of the devices are then converted to the corresponding Y-parameters using MATLAB software with characteristic impedance of 50 Ω. Thus, the measured Y-parameters of all devices are available in the sampled data form of equation (17). Based on the Y-parameter data, the conventional SSEC model with constant circuit elements (Fig. 1) and the proposed frequency dependent SSEC

model are realized. The procedure to extract constant circuit element values of the conventional SSEC model is detailed in [13], [14]. The values of individual circuit elements of conventional constant value SSEC model for all the AlGaN/GaN MOS-HEMT structures of this work are provided in Table A1 of the Appendix section.

V. RESULTS AND DISCUSSION

A. ACCURACY COMPARISON BETWEEN CONVENTIONAL SSEC MODEL AND PROPOSED FREQUENCY DEPENDENT SSEC MODEL

From the measured S-parameters of AlGaN/GaN MOS-HEMTs, both the conventional SSEC model (Fig. 1) and the proposed frequency dependent SSEC model are developed using the methodology described in Section II-A and Section III, respectively. For the frequency dependent SSEC model, the individual circuit elements are represented using polynomial functions of frequency where the order K of the functions are progressively varied from the 0^{th} order to 5^{th} order. Note that the 0^{th} order polynomial function automatically refers to the conventional SSEC model of Fig. 1. For the polynomial functions of different orders, the Y-parameters of the AlGaN/GaN MOS-HEMT devices are recovered using equation (20). Thereafter, the L2 error norm between the recovered Y-parameters of equation (20) and the measured Y-parameters of equation (17) are quantified as [31], [32]:

$$L_{\alpha\beta} = \frac{\sqrt{\sum_{u=1}^{n}\left(Y_{\alpha\beta}(data)_u - Y_{\alpha\beta}(\mathrm{model})_u\right)^2}}{N} \qquad (21)$$

where $L_{\alpha\beta}$ is the L2 error norm for the entry in the (α, β) position of the Y-parameter matrix. The values of the L2 error norm calculated using equation (21) for the AlGaN/GaN MOS-HEMTs with SiO_2 and Al_2O_3 as gate dielectrics (L_G = 1.5 μm) are shown in Fig. 4. In particular, Fig. 4 (a)-(d) illustrates the calculated L2 error norms for Y_{11}, Y_{12}, Y_{21}, and Y_{22}, respectively. It is noted from Fig. 4 that by increasing the order of the polynomial functions (K), the value of the L2 error norm decreases. Importantly, it is observed that as the order increases from K = 0 (i.e., the conventional SSEC model of Fig. 1) to K = 2, there is nearly an order of magnitude decrease in the error norm for most of the Y-parameters.

However, increasing the order of the polynomial functions beyond K = 2 does not significantly improve the L2 error norm any further. This indicates a diminishing return on accuracy by increasing the order of the polynomial functions. A similar trend is also observed for AlGaN/GaN MOS-HEMTs having SiO_2 and Al_2O_3 as gate dielectric having L_G = 2 μm, shown in Fig. A1 of the Appendix section. Thus, a 2^{nd} order polynomial function representation of the circuit elements of the SSEC model is considered to provide a sufficiently accurate fit for the proposed frequency dependent SSEC element model. The observed values of the L2 error norm for the 0^{th} order polynomials (i.e., the conventional SSEC model of Fig. 1) and the 2^{nd} order polynomials (i.e., the proposed frequency dependent SSEC model) for all the AlGaN/GaN MOS-HEMTs used in this study is recorded in Table 1. From the data of Table 1, it is clear that the proposed model is significantly more accurate than the conventional SSEC model (Fig. 1) having constant element values.

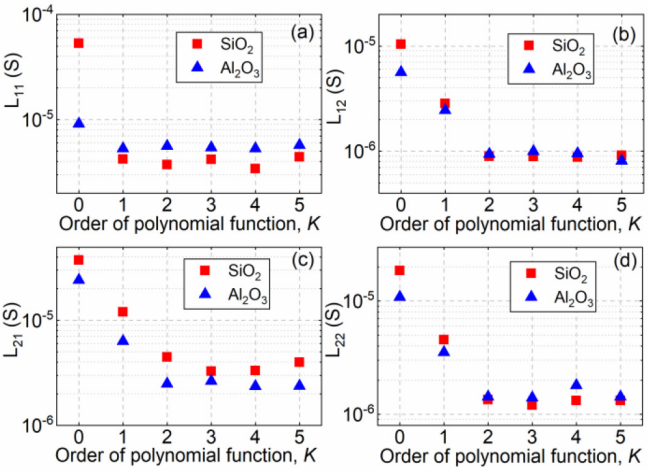

FIGURE 4. L2 error norm of AlGaN/GaN MOS-HEMTs for different gate dielectrics (L_G = 1.5 μm). (a)-(d) are L_{11}, L_{12}, L_{21}, and L_{22}, respectively for different order of polynomial functions (K).

TABLE 1. L2 error norm for Y-parameters of AlGaN/GaN MOS-HEMTs with different gate dielectric and gate length.

Gate dielectric and L_G of AlGaN/GaN MOS-HEMT	Order of the polynomial (K)	L_{11}	L_{12}	L_{21}	L_{22}
		($\times 10^{-6}$ S)			
Dielectric: SiO_2 L_G = 1.5 μm	0	52.9	10.4	37.3	18.5
	2	3.73	8.92	4.46	1.53
Dielectric: SiO_2 L_G = 2 μm	0	25.9	15.2	18.9	20.5
	2	2.66	1.14	3.68	2.77
Dielectric: Al_2O_3 L_G = 1.5 μm	0	9.08	5.6	24	10.8
	2	5.6	0.93	2.47	1.42
Dielectric: Al_2O_3 L_G = 2 μm	0	63	10.9	6.65	20.4
	2	3.81	2.34	4.4	3.33

The large L2 error norm observed for the conventional SSEC model (Fig. 1) in Table 1 is attributed to the inherent variation in the lumped circuit element values at high frequencies, as reported by other authors (see Section II-B). Figure 5 (a)–(h) clearly illustrates this inherent variation in the values of the circuit elements R_i, R_{gd}, g_{ds}, g_m, C_{gs}, C_{ds}, C_{gd} and τ, respectively, as calculated from the experimentally measured Y-parameter data for the AlGaN/GaN MOS-HEMT having SiO_2 as gate dielectric and L_G = 1.5 μm. Moreover, the constant circuit element values derived from the Y-parameters using equations (4)-(11) for the conventional SSEC model (Fig. 1) and the proposed frequency dependent SSEC model using 2^{nd} order polynomials are also displayed in Fig. 5. From the comparison of Fig. 5, it is clear that all the lumped circuit element

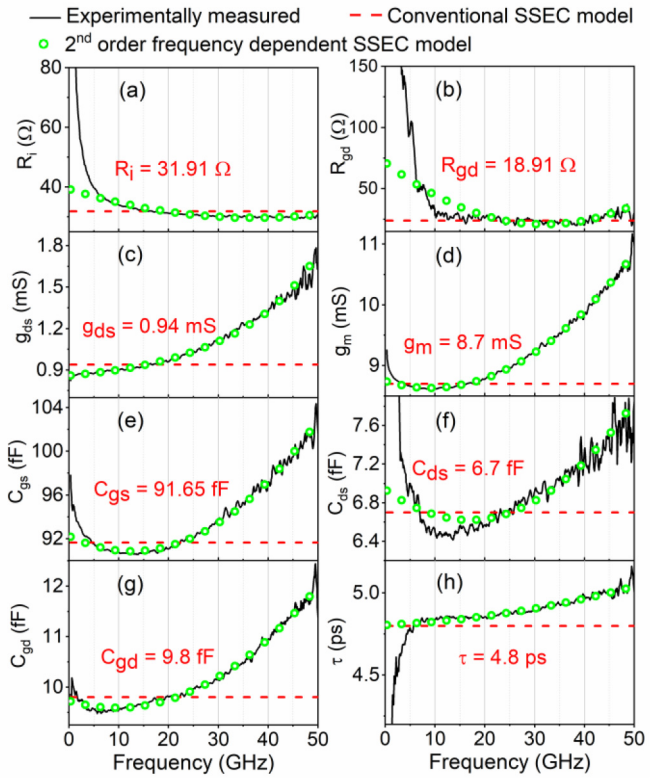

FIGURE 5. Variations of the SSEC model circuit elements with frequency for AlGaN/GaN MOSHEMT having SiO_2 as gate dielectric ($L_G = 1.5\ \mu m$); (a)-(h) shows the variations in R_i, R_{gd}, g_{ds}, g_m, C_{gs}, C_{ds}, C_{gd} and τ, respectively.

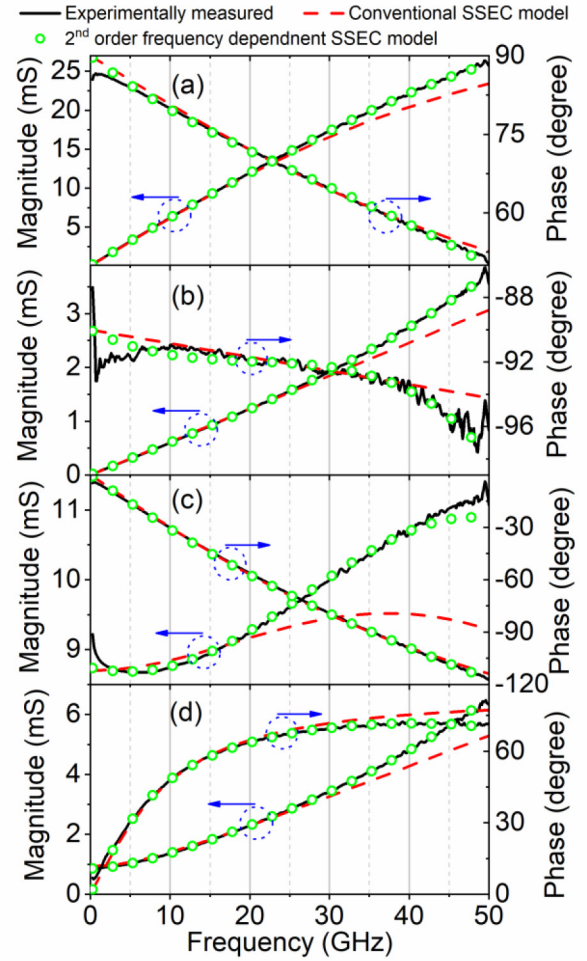

FIGURE 6. Y-parameters of AlGaN/GaN MOS-HEMT with SiO_2 as gate dielectric ($L_G = 1.5\ \mu m$); (a)-(d) shows Y_{11}, Y_{12}, Y_{21} and Y_{22}, respectively.

values vary with frequency of measurement. Thus, assuming constant values of these lumped circuit elements, as in the conventional SSEC model of Fig. 1, leads to significant deviation from the corresponding experimentally measured values. Especially at frequency beyond ~20 GHz, device transconductances (g_{ds} and g_m) and device capacitances (C_{gs}, C_{ds} and C_{gd}) are observed to be strong functions of frequency, as shown in Fig. 5 (c)–(g) respectively. Therefore, considering these circuit element values to be constant in the SSEC model of Fig. 1 is expected to result in a large L2 error norm when compared with the experimentally measured Y-parameters.

On contrary, considering the circuit element values to be functions of frequency is necessary to better fit the experimentally measured data to the SSEC model, especially beyond 20 GHz. As observed in Fig. 5, considering all the circuit element to be 2nd order function of frequency promises sufficient accuracy, as expected from Fig. 4. A similar trend is also observed for all AlGaN/GaN MOS-HEMTs investigated in this work; corresponding graphs for AlGaN/GaN MOS-HEMT having Al_2O_3 gate dielectric and $L_G = 1.5\ \mu m$ is shown in Fig. A2 of the Appendix section. Thus, a lower error between the experimentally observed data and SSEC model is obtained by considering all the circuit elements to be 2nd order polynomial functions of frequency. A higher order polynomial function representation for the lumped circuit elements may be necessary for AlGaN/GaN MOS-HEMTs with shorter channel lengths and higher frequency of measurements. At this point, further studies are necessary to determine exact reasons behind the non-linear change in lumped circuit element values with an increase in frequency of measurement.

Next, the comparison of the Y-parameters predicted by the conventional SSEC model (Fig. 1) and the proposed frequency dependent SSEC model using 2nd order polynomials for AlGaN/GaN MOS-HEMT with SiO_2 gate dielectric ($L_G = 1.5\ \mu m$) up to 50 GHz is shown in Fig. 6. Experimentally measured Y-parameter data is also included in Fig. 6 and had a bias condition of $V_{GS} = -5$ V and $V_{DS} = 15$ V. The corresponding graphs for AlGaN/GaN MOS-HEMT with Al_2O_3 gate dielectric ($L_G = 1.5\ \mu m$) is shown in Fig. A3 of the Appendix section. Interestingly, the conventional SSEC model of Fig. 1 is observed to closely match the phase of experimentally measured Y-parameters. However, this comes at the cost of a significant deviation in magnitude of Y-parameters beyond ~ 20 GHz – something

that is not seen using the proposed frequency dependent SSEC model. Similar results are also observed between the experimentally measured data and the predicted data for AlGaN/GaN MOS-HEMT with Al_2O_3 as gate dielectric and varying channel lengths (images shown in the Appendix section). Therefore, Fig. 6 clearly demonstrates the improved accuracy provided by the frequency dependent SSEC model over the conventional SSEC model of Fig. 1 at millimeter wave frequencies.

B. GAIN ANALYSIS FOR CONVENTIONAL SSEC MODEL AND FREQUENCY DEPENDENT SSEC MODEL

In Section III-A, the improvement in accuracy provided by the proposed frequency dependent SSEC model over the conventional SSEC model of Fig. 1 for AlGaN/GaN MOS-HEMT devices has been verified. This improvement in accuracy translates to improvement in estimating the unity gain frequency (f_t) and maximum frequency of oscillation (f_{max}) of the devices. Traditionally, f_t and f_{max} are derived from the current gain (H_{21}) and unilateral gain (U) given as [33]:

$$H_{21} = \frac{-2S_{21}}{(1-S_{11})(1+S_{22})+S_{12}S_{21}} \tag{22}$$

$$U = \frac{\left|\frac{S_{21}}{S_{12}}-1\right|^2}{2\chi\left|\frac{S_{21}}{S_{12}}\right| - 2Re\left(\frac{S_{21}}{S_{12}}\right)} \tag{23}$$

where S_{11}, S_{12}, S_{21}, and S_{22} represents the S-parameters of the AlGaN/GaN MOS-HEMT, and

$$\chi = \frac{1-|S_{11}|^2-|S_{22}|^2+|S_{11}S_{22}-S_{12}S_{21}|^2}{2|S_{12}S_{21}|}. \tag{24}$$

The x-intercept of $20log(|H_{21}|)$ vs frequency plot and $20log(|U|)$ vs frequency plot yields the values of f_t and f_{max}, respectively. The S-parameters predicted by the conventional SSEC model of Fig. 1 is derived from the predicted Y-parameters obtained from equation (2). Similarly, the S-parameters predicted by the frequency dependent SSEC model is derived from the predicted Y-parameters obtained from equation (20).

Next, the quantities H_{21} and U are calculated from the experimentally measured data, the conventional SSEC model of Fig. 1, and the proposed frequency dependent SSEC model for the AlGaN/GaN MOS-HEMT devices (SiO_2 and Al_2O_3 gate dielectric, $L_G = 1.5$ μm) are displayed in Fig. 7. For the frequency range of 300 MHz to ~10 GHz, the slope of $20log(|H_{21}|)$ vs frequency plot is ~20 dB indicating negligible frequency dispersion, as observed in Fig. 7 (a) and (c). However, for frequency above 10 GHz, the values of the corresponding slope increases indicating a high frequency capacitance dispersion. This increased slope is far better captured by the proposed frequency dependent SSEC model than the conventional SSEC model of Fig. 1 as can be observed in the insets of Fig. 7 (a) and Fig. 7 (c). Recent reports also indicate a similar failure of constant value

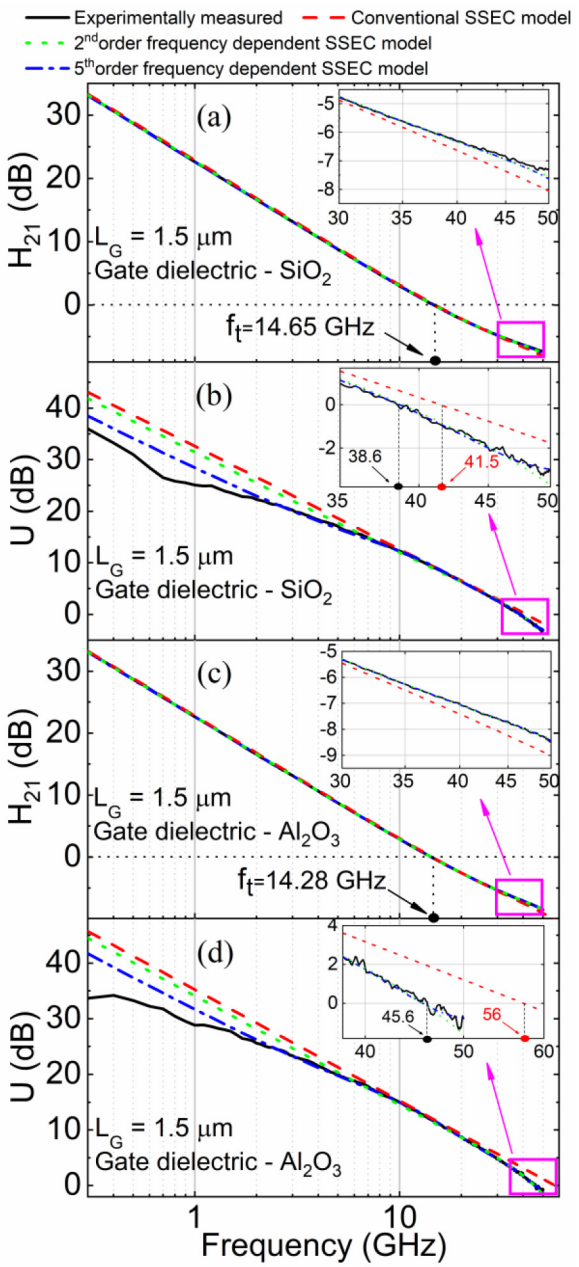

FIGURE 7. Gain plots for AlGaN/GaN MOS-HEMTs: (a) and (c) show the variations in H_{21}; and (b) and (d) show the variations in U with frequency.

lumped element based SSEC models to fit the experimentally measured H_{21} values in AlGaN/GaN HEMTs having high f_t and f_{max} values [34]. Furthermore, the values of f_{max} (which lie beyond f_t in the higher frequency range) is largely over-estimated by the conventional SSEC model of Fig. 1 for all the AlGaN/GaN MOS-HEMTs under investigation, corresponding graphs for AlGaN/GaN MOS-HEMTs with SiO_2 and Al_2O_3 gate dielectric ($L_G = 1.5$ μm) are shown in Fig. 7 (b) and (d), respectively. On contrary, the proposed frequency dependent SSEC model shows very good agreement with the experimentally measured data when estimating f_{max}.

TABLE 2. Values of Ft and Fmax calculated for AlGaN/GaN MOS-HEMT having different gate dielectric and gate length.

Devices	Y-parameters	f_t (GHz)	f_{max} (GHz)
Dielectric: SiO_2 L_G = 1.5 µm	Experimentally measured	14.65	38.6
	Conventional SSEC model	14.9	41.5
	Frequency dependent SSEC model (K=2)	14.63	40
Dielectric: SiO_2 L_G = 2 µm	Experimentally measured	9.76	29.6
	Conventional SSEC model	9.94	32.4
	Frequency dependent SSEC model (K=2)	9.75	29.35
Dielectric: Al_2O_3 L_G = 1.5 µm	Experimentally measured	14.28	45.6
	Conventional SSEC model	14.5	56
	Frequency dependent SSEC model (K=2)	14.33	45
Dielectric: Al_2O_3 L_G = 2 µm	Experimentally measured	10.01	40.4
	Conventional SSEC model	10	45.96
	Frequency dependent SSEC model (K=2)	10	41.5

TABLE A.I. Conventional SSEC model elements values extracted from experimentally measured data for AlGaN/GaN MOS-HEMTs.

Intrinsic elements	SiO_2		Al_2O_3	
	L_G=1.5 µm	L_G=2 µm	L_G=1.5 µm	L_G=2 µm
C_{gs} (fF)	91.65	111.6	135.6	140
C_{gd} (fF)	9.80	10	9.66	8
C_{ds} (fF)	6.7	5.95	6.8	5
g_m (mS)	8.7	7.2	12.5	9
g_{ds} (mS)	0.94	0.75	0.76	0.5
R_i (Ω)	31.91	34.4	21.63	24
R_{dg} (Ω)	18.91	18.19	2	4
τ (ps)	4.8	6.5	4.8	6.2

The ability of the proposed frequency dependent SSEC model to outperform the conventional SSEC model of Fig. 1 is also evident from the calculated values of f_t and f_{max} as listed in Table 2. From Table 2, it is seen that the error in the value of f_{max} estimated by the conventional SSEC model of Fig. 1 is as high as ∼18.6% for AlGaN/GaN MOS-HEMT having Al_2O_3 dielectric and $L_G = 1.5$ µm. Such a large error in estimation is not acceptable for high frequency application. On contrary, the values of f_t and f_{max} estimated by the proposed frequency dependent SSEC model using a 2nd order polynomial function closely matches the experimentally measured f_t and f_{max} values. Increasing the order of the polynomial function better fits the experimentally measured values at lower frequency as well as higher frequency, as shown in Fig. 7. Note that the experimentally measured S-parameters in this work is up to 50 GHz; a higher order polynomial function may be necessary if the f_t and/or f_{max} values are further extended beyond this 50 GHz range. Thus, representing all the SSEC model elements of AlGaN/GaN MOS-HEMTs as a function of frequency is necessary to correctly fit the experimentally measured S-parameters and better estimate f_t and f_{max} values.

C. DISCUSSION

The results shown in Sections V-A and V-B indicate that the frequency dependent SSEC model proposed in this work is a generic model that can be applied to any electronic device (such as MOSFETs, multi-finger HEMTs or fin-FETs [11], [35], MOS-HEMTs, etc.) whose SSEC resembles the topology shown in Fig. 1. The end user is required to find the maximum order of the polynomial functions representing the SSEC model circuit elements that best fits the experimentally measured Y-parameters. Typically, this order is small as seen from these examples. In contrast, if the Y-parameters are directly expressed as polynomials functions of frequency and the coefficients are calculated using equation (18), then a much larger order would be required. Moreover, the resultant matrix A equivalent to equation (18) will be highly ill-conditioned. Consequently, calculating the inverse of A^TA will be highly inaccurate, and in many cases, downright impossible [36], [37]. Thus, directly representing the Y-parameters in terms of polynomial function is not a valid alternative to the proposed model.

It is noted that the dependency of C_{gs} or C_{gd} values with respect to frequency is obtained from experimentally measured Y-parameters. This dependency is due to both dispersive effects as well as the effect of residual parasitics that may not have been completely removed during de-embedding. For the chosen examples of this work, this dependency seems linear in the high frequency region. However, such dependency may not necessarily remain linear as we further increase the frequency or vary the AlGaN/GaN MOS-HEMT device geometry. For other circuit elements, especially resistive/conductive circuit elements, dielectric losses and residual capacitive/inductive parasitics are responsible for the variation of their values with respect to frequency. Now, it is observed from Fig. 5 that different circuit elements show different levels and trajectories of variation with respect to frequency. Thus, to capture this different level of variation and trajectories, different orders of polynomials can also be adopted for different circuit elements.

Furthermore, as observed in Fig. 6, both the conventional SSEC model and frequency dependent SSEC model fail to capture some of the Y-parameter variations at broadband frequency range, especially in the low frequency region. This indicates that the conventional SSEC model of Fig. 1 may require minor modifications such as addition of inductive and/or capacitive elements to better capture the AlGaN/GaN MOS-HEMT behavior over broadband frequency range. However, such modification invalidates the expression of the Y-parameters in equation (2) and the

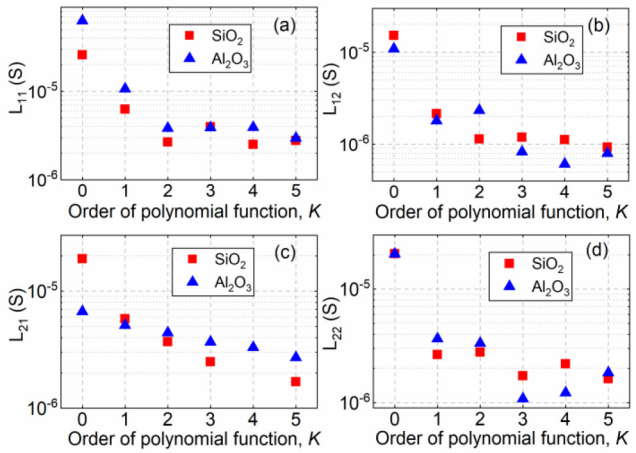

FIGURE A.I. **L2 error norm of AlGaN/GaN MOS-HEMTs for different gate dielectrics ($L_G = 2\ \mu$m). (a)-(d) are L_{11}, L_{12}, L_{21} and L_{22}, respectively for different order of polynomial functions (K).**

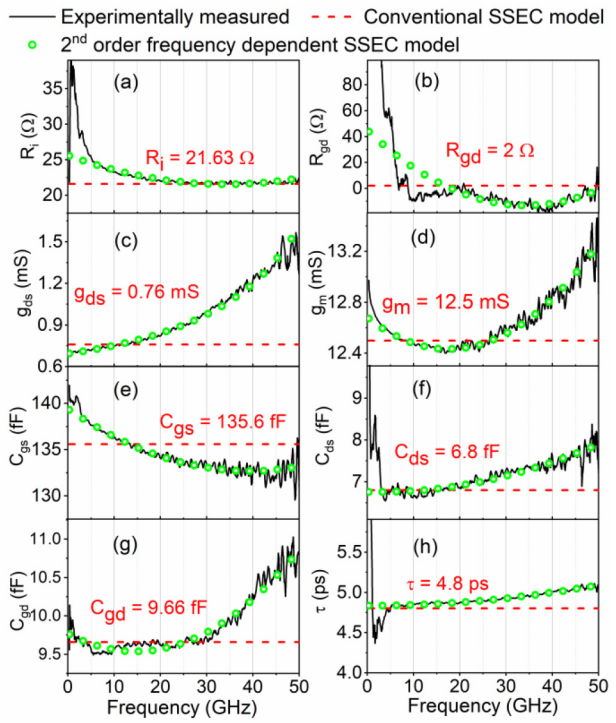

FIGURE A.II. **Variations of the SSEC model circuit elements with frequency for AlGaN/GaN MOS-HEMTs ($L_G = 1.5\ \mu$m) having Al_2O_3 as gate dielectric and; (a)-(h) shows the variations in R_i, R_{gd}, g_{ds}, g_m, C_{gs}, C_{ds}, C_{gd} and τ, respectively.**

closed-form equations of equation (4)-(11). This work is dedicated to correctly predict the Y-parameters using the conventional SSEC model topology of Fig. 1. Hence any modification to the conventional SSEC model of Fig. 1 is avoided in this work.

VI. CONCLUSION

Traditionally used lumped small signal equivalent circuit models for AlGaN/GaN metal oxide semiconductor high electron mobility transistors (MOS-HEMTs) implicitly assume the values of the circuit elements to be constant. Thus, these models fail to capture the variability in the circuit element values at high frequencies resulting in low model accuracy. Therefore, in this work, a modified lumped small signal equivalent circuit model is proposed where the value of the circuit elements making up the model are treated as frequency dependent polynomial functions. This frequency dependent lumped element small signal equivalent circuit model can better capture the experimentally measured Y-parameters of AlGaN/GaN MOS-HEMTs, especially in the high frequency region (i.e., greater than 20 GHz). Moreover, in this work, a least-squares based curve-fitting approach has been developed to offline estimate the coefficients of the polynomials from the experimentally measured Y-parameter data. The proposed model is sufficiently generic and can be applied to different devices such as MOSFETs, HEMTs, and MOS-HEMTs by varying the order of the polynomial function appropriately.

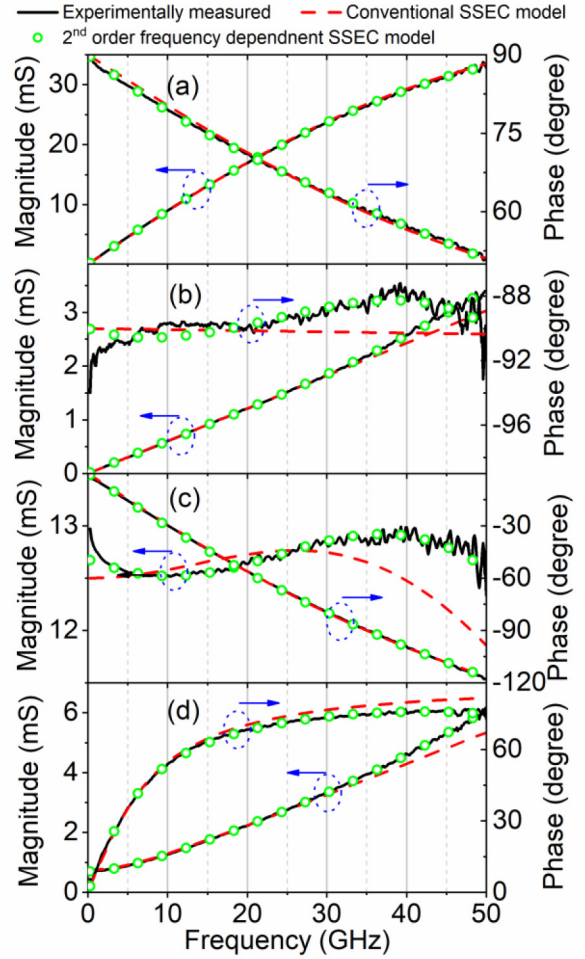

FIGURE A.III. **Y-parameters of AlGaN/GaN MOS-HEMT with Al_2O_3 as gate dielectric ($L_G = 1.5\ \mu$m); (a)-(d) shows Y_{11}, Y_{12}, Y_{21} and Y_{22}, respectively.**

APPENDIX

Appendix section consist of Table A.I, Fig. A.I, Fig. A.II, and Fig. A.III. Table A1 lists the values of all circuit elements derived for the conventional SSEC model for AlGaN/GaN MOS-HEMTs having different gate dielectrics and L_G.

Figure A.I highlights the values of the L2 error norm calculated using equation (21) for the AlGaN/GaN MOS-HEMTs with SiO_2 and Al_2O_3 as gate dielectrics ($L_G = 2$ μm).

Similarly, Fig. A.II represents the variations in the values of circuit elements of the conventional SSEC model with frequency for AlGaN/GaN MOS-HEMT having Al_2O_3 as gate dielectric (L_G = 1.5 μm).

Finally, Fig. A.III illustrates the comparison of the Y-parameters predicted by the conventional SSEC model (Fig. 1) and the proposed frequency dependent SSEC model using 2nd order polynomials for AlGaN/GaN MOS-HEMT with Al_2O_3 gate dielectric ($L_G = 1.5$ μm) up to 50 GHz.

REFERENCES

[1] R. Sun, J. Lai, W. Chen, and B. Zhang, "GaN power integration for high frequency and high efficiency power applications: A review," *IEEE Access*, vol. 8, pp. 15529–15542, 2020, doi: 10.1109/ACCESS.2020.2967027.

[2] J. J. Komiak, "GaN HEMT: Dominant force in high-frequency solid-state power amplifiers," *IEEE Microw. Mag.*, vol. 16, no. 3, pp. 97–105, Apr. 2015, doi: 10.1109/MMM.2014.2385303.

[3] V. Sandeep, J. C. Pravin, A. R. Babu, and P. Prajoon, "Impact of AlInN back-barrier over AlGaN/GaN MOS-HEMT with HfO2 dielectric using cubic spline interpolation technique," *IEEE Trans. Electron Devices*, vol. 67, no. 9, pp. 3558–3563, Sep. 2020, doi: 10.1109/TED.2020.3010710.

[4] C.-T. Lee, Y.-L. Chiou, and C.-S. Lee, "AlGaN/GaN MOS-HEMTs with gate ZnO dielectric layer," *IEEE Electron Device Lett.*, vol. 31, no. 11, pp. 1220–1223, Nov. 2010, doi: 10.1109/LED.2010.2066543.

[5] K. Geng, D. Chen, Q. Zhou, and H. Wang, "AlGaN/GaN MIS-HEMT with PECVD SiNx, SiON, SiO2 as gate dielectric and passivation layer," *Electronics*, vol. 7, no. 12, Art. no. 416, Dec. 2018, doi: 10.3390/electronics7120416.

[6] E. Miyazaki, Y. Goda, S. Kishimoto, and T. Mizutani, "Comparative study of AlGaN/GaN metal-oxide-semiconductor heterostructure field-effect transistors with Al_2O_3 and HfO_2 gate oxide," *Solid-State Electron.*, vol. 62, no. 1, pp. 152–155, Aug. 2011, doi: 10.1016/j.sse.2011.04.017.

[7] Y. C. Chang *et al.*, "Atomic-layer-deposited Al_2O_3 and HfO_2 on GaN: A comparative study on interfaces and electrical characteristics," *Microelectron. Eng.*, vol. 88, no. 7, pp. 1207–1210, Jul. 2011, doi: 10.1016/j.mee.2011.03.098.

[8] T. J. Brazil, "Simulating circuits and devices," *IEEE Microw. Mag.*, vol. 4, no. 1, pp. 42–50, Mar. 2003, doi: 10.1109/MMW.2003.1188235.

[9] Y. Karisan, C. Caglayan, G. C. Trichopoulos, and K. Sertel, "Lumped-element equivalent-circuit modeling of millimeter-wave HEMT parasitics through full-wave electromagnetic analysis," *IEEE Trans. Microw. Theory Techn.*, vol. 64, no. 5, pp. 1419–1430, May 2016, doi: 10.1109/TMTT.2016.2549520.

[10] G. Crupi *et al.*, "High-frequency extraction of the extrinsic capacitances for GaN HEMT technology," *IEEE Microw. Compon. Lett.*, vol. 21, no. 8, pp. 445–447, Aug. 2011, doi: 10.1109/LMWC.2011.2160525.

[11] G. Crupi, A. Raffo, G. Avolio, D. M. M.-P. Schreurs, G. Vannini, and A. Caddemi, "Temperature influence on GaN HEMT equivalent circuit," *IEEE Microw. Compon. Lett.*, vol. 26, no. 10, pp. 813–815, Oct. 2016, doi: 10.1109/LMWC.2016.2601487.

[12] C. Pavageau *et al.*, "A 7-dB 43-GHz CMOS distributed amplifier on high-resistivity SOI substrates," *IEEE Trans. Microw. Theory Techn.*, vol. 56, no. 3, pp. 587–598, Mar. 2008, doi: 10.1109/TMTT.2008.916930.

[13] S. A. Ahsan, S. Ghosh, S. Khandelwal, and Y. S. Chauhan, "Physics-based multi-bias RF large-signal GaN HEMT modeling and parameter extraction flow," *IEEE J. Electron Devices Soc.*, vol. 5, no. 5, pp. 310–319, Sep. 2017, doi: 10.1109/JEDS.2017.2724839.

[14] I. Kwon, M. Je, K. Lee, and H. Shin, "A simple and analytical parameter-extraction method of a microwave MOSFET," *IEEE Trans. Microw. Theory Techn.*, vol. 50, no. 6, pp. 1503–1509, Jun. 2002, doi: 10.1109/TMTT.2002.1006411.

[15] V. Kilchytska *et al.*, "Frequency variation of the small-signal output conductance of decananometer MOSFETs due to substrate crosstalk," *IEEE Electron Device Lett.*, vol. 28, no. 5, pp. 419–421, May 2007, doi: 10.1109/LED.2007.895374.

[16] R. Valentin *et al.*, "RF small-signal analysis of Schottky-barrier p-MOSFET," *IEEE Trans. Electron Devices*, vol. 55, no. 5, pp. 1192–1202, May 2008, doi: 10.1109/TED.2008.919382.

[17] R. G. Brady, C. H. Oxley, and T. J. Brazil, "An improved small-signal parameter-extraction algorithm for GaN HEMT devices," *IEEE Trans. Microw. Theory Techn.*, vol. 56, no. 7, pp. 1535–1544, Jul. 2008, doi: 10.1109/TMTT.2008.925212.

[18] Y. Wu, Q. Wang, J. Liu, C. Zhao, H. Tang, and K. Kang, "An improved small-signal equivalent circuit model considering channel current magnetic effect," *IEEE Microw. Compon. Lett.*, vol. 28, no. 9, pp. 804–806, Sep. 2018, doi: 10.1109/LMWC.2018.2850895.

[19] R. Sung, P. Bendix, and M. B. Das, "Extraction of high-frequency equivalent circuit parameters of submicron gate-length MOSFET's," *IEEE Trans. Electron Devices*, vol. 45, no. 8, pp. 1769–1775, Aug. 1998, doi: 10.1109/16.704377.

[20] Y. Tang, L. Zhang, and Y. Wang, "Accurate small signal modeling and extraction of silicon MOSFET for RF IC application," *Solid-State Electron.*, vol. 54, no. 11, pp. 1312–1318, Nov. 2010, doi: 10.1016/j.sse.2010.06.025.

[21] F. Y. Huang, X. S. Tang, Z. N. Wei, L. H. Zhang, and N. Jiang, "An improved small-signal equivalent circuit for GaN high-electron mobility transistors," *IEEE Electron Device Lett.*, vol. 37, no. 11, pp. 1399–1402, Nov. 2016, doi: 10.1109/LED.2016.2609462.

[22] A. Jarndal and G. Kompa, "A new small-signal modeling approach applied to GaN devices," *IEEE Trans. Microw. Theory Techn.*, vol. 53, no. 11, pp. 3440–3448, Nov. 2005, doi: 10.1109/TMTT.2005.857332.

[23] J. R. Shealy, J. Wang, and R. Brown, "Methodology for small-signal model extraction of AlGaN HEMTs," *IEEE Trans. Electron Devices*, vol. 55, no. 7, pp. 1603–1613, Jul. 2008, doi: 10.1109/TED.2008.925335.

[24] W.-B. Tang, C.-M. Wang, and Y.-M. Hsin, "A new extraction technique for the complete small-signal equivalent-circuit model of InGaP/GaAs HBT including base contact impedance and AC current crowding effect," *IEEE Trans. Microw. Theory Techn.*, vol. 54, no. 10, pp. 3641–3647, Oct. 2006, doi: 10.1109/TMTT.2006.882411.

[25] N. Rorsman, M. Garcia, C. Karlsson, and H. Zirath, "Accurate small-signal modeling of HFET's for millimeter-wave applications," *IEEE Trans. Microw. Theory Techn.*, vol. 44, no. 3, pp. 432–437, Mar. 1996, doi: 10.1109/22.486152.

[26] D.-Z. Feng, Z. Bao, and L.-C. Jiao, "Total least mean squares algorithm," *IEEE Trans. Signal Process.*, vol. 46, no. 8, pp. 2122–2130, Aug. 1998, doi: 10.1109/78.705421.

[27] Q. Fan, J. H. Leach, and H. Morkoc, "Small signal equivalent circuit modeling for AlGaN/GaN HFET: Hybrid extraction method for determining circuit elements of AlGaN/GaN HFET," *Proc. IEEE*, vol. 98, no. 7, pp. 1140–1150, Jul. 2010, doi: 10.1109/JPROC.2010.2044630.

[28] Y. Cao, W. Zhang, J. Fu, Q. Wang, L. Liu, and A. Guo, "A complete small-signal MOSFET model and parameter extraction technique for millimeter wave applications," *IEEE J. Electron Devices Soc.*, vol. 7, pp. 398–403, 2019, doi: 10.1109/JEDS.2019.2900202.

[29] L. F. Tiemeijer, R. J. Havens, A. B. M. Jansman, and Y. Bouttement, "Comparison of the 'pad-open-short' and 'open-short-load' deembedding techniques for accurate on-wafer RF characterization of high-quality passives," *IEEE Trans. Microw. Theory Techn.*, vol. 53, no. 2, pp. 723–729, Feb. 2005, doi: 10.1109/TMTT.2004.840621.

[30] J. Luo, L. Zhang, and Y. Wang, "A distributed de-embedding solution for CMOS mm-Wave on-wafer measurements based-on double open-short technique," *IEEE Microw. Compon. Lett.*, vol. 23, no. 12, pp. 686–688, Dec. 2013, doi: 10.1109/LMWC.2013.2284773.

[31] Y. Liu, Q. Gao, X. Gao, and L. Shao, "L_2,1-norm discriminant manifold learning," *IEEE Access*, vol. 6, pp. 40723–40734, 2018, doi: 10.1109/ACCESS.2018.2859299.
[32] R. Wang, J. Han, B. F. Cockburn, and D. G. Elliott, "Stochastic circuit design and performance evaluation of vector quantization for different error measures," *IEEE Trans. Very Large Scale Integr. (VLSI) Syst.*, vol. 24, no. 10, pp. 3169–3183, Oct. 2016, doi: 10.1109/TVLSI.2016.2535313.
[33] D. M. Pozer, *Microwave Engineering*, 4th ed. Hoboken, NJ, USA: Wiley, 2011.
[34] K. Shinohara *et al.*, "Scaling of GaN HEMTs and schottky diodes for submillimeter-wave MMIC applications," *IEEE Trans. Electron Devices*, vol. 60, no. 10, pp. 2982–2996, Oct. 2013, doi: 10.1109/TED.2013.2268160.
[35] G. Crupi, D. Schreurs, B. Parvais, A. Caddemi, A. Mercha, and S. Decoutere, "Scalable and multibias high frequency modeling of multi-fin FETs," *Solid-State Electron.*, vol. 50, nos. 11–12, pp. 1780–1786, Nov. 2006, doi: 10.1016/j.sse.2006.09.006.
[36] W. T. Beyene and J. Schutt-Aine, "Accurate frequency-domain modeling and efficient circuit simulation of high-speed packaging interconnects," *IEEE Trans. Microw. Theory Techn.*, vol. 45, no. 10, pp. 1941–1947, Oct. 1997, doi: 10.1109/22.641798.
[37] W. T. Beyene and J. E. Schutt-Aine, "Efficient transient simulation of high-speed interconnects characterized by sampled data," *IEEE Trans. Compon., Packag., Manuf. Technol. B*, vol. 21, no. 1, pp. 105–114, Feb. 1998, doi: 10.1109/96.659513.